SUPPORTING INFORMATION

Molecular Tuning in Highly Fluorescent Dithieno[3,2-*b*:2',3'-*d*]pyrrole-based Oligomers: Effects of N-Functionalization and Terminal Aryl Unit

Sean J. Evenson,[a] Ted M. Pappenfus,[b] M. Carmen Ruiz Delgado,[c] Karla R. Radke-Wohlers,[a] J. T. López Navarrete,[c] and Seth C. Rasmussen*[a]

[a]*Department of Chemistry and Biochemistry, North Dakota State University, NDSU Dept. 2735, P.O. Box 6050, Fargo, ND 58108-6050, United States. Fax: 1-701-231-8747; Tel: 1-701-231-8831; E-mail: seth.rasmussen@ndsu.edu*

[b]*Division of Science and Mathematics, University of Minnesota, Morris, MN 56267, United States. Fax: +1 320 589-6371; Tel: +1 320 589-6340; E-mail: pappe001@morris.umn.edu*

[c]*Department of Physical Chemistry, University of Málaga, Campus de Teatinos s/n, Málaga 29071, Spain. Email: carmenrd@uma.es*

Table of Contents:

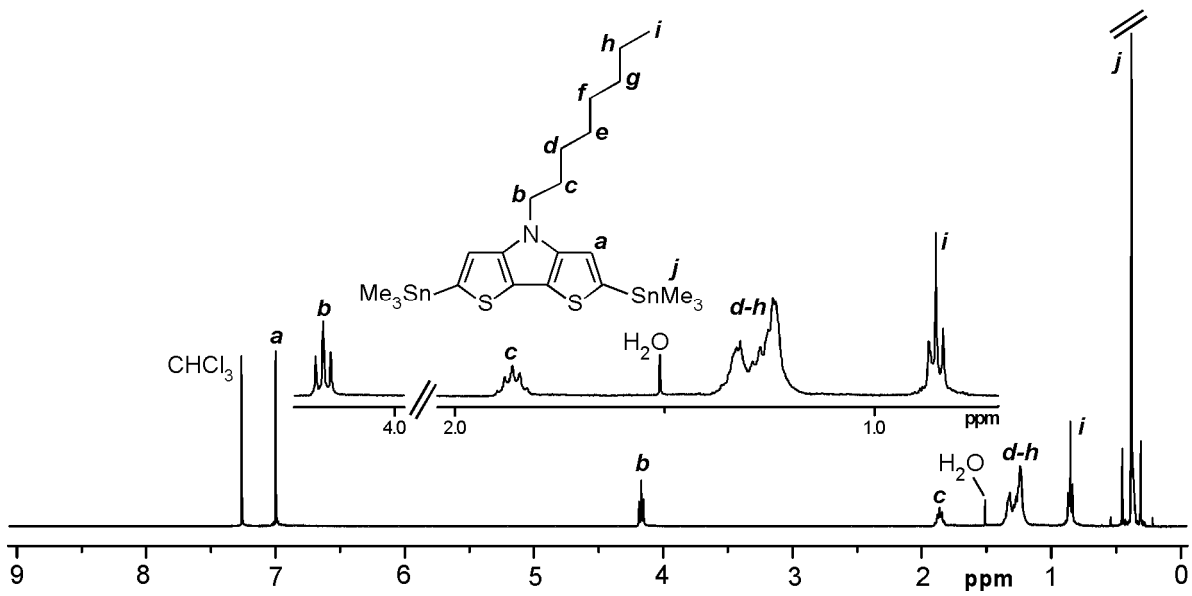

Figure S1. ^{1}H NMR Spectrum of Compound **14a**

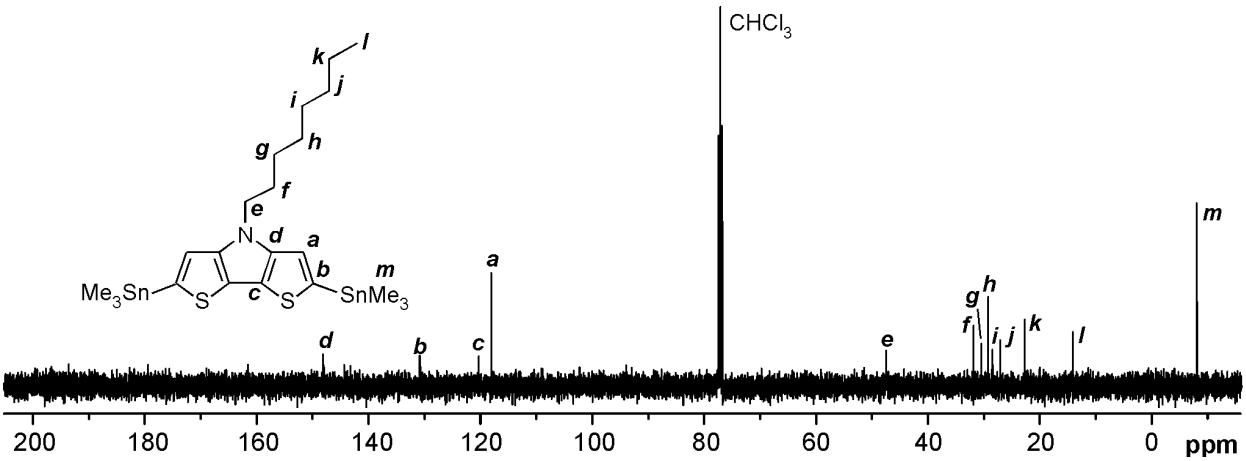

Figure S2. ^{13}C NMR Spectrum of Compound **14a**

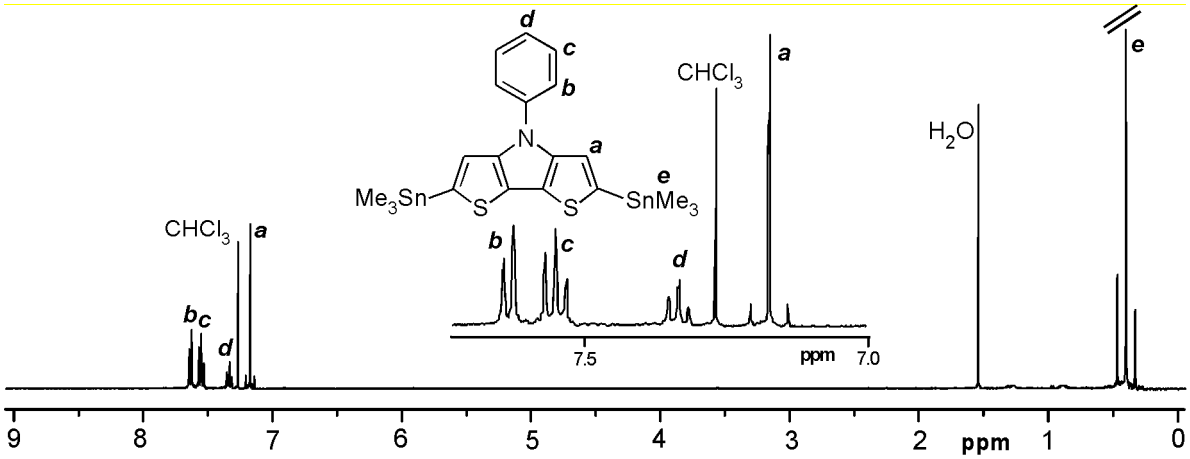

Figure S3. ^{1}H NMR Spectrum of Compound **14b**

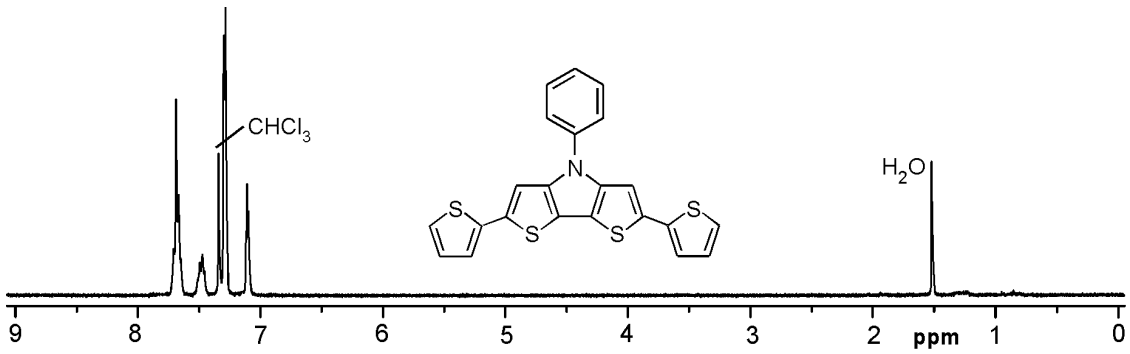

Figure S4. ^{1}H NMR Spectrum of Compound **7b**

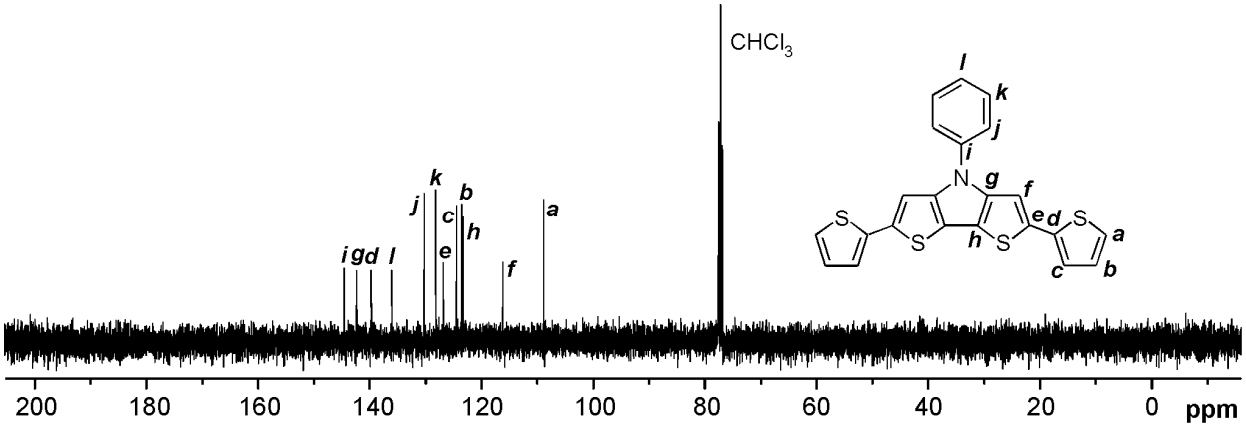

Figure S5. ^{13}C NMR Spectrum of Compound **7b**

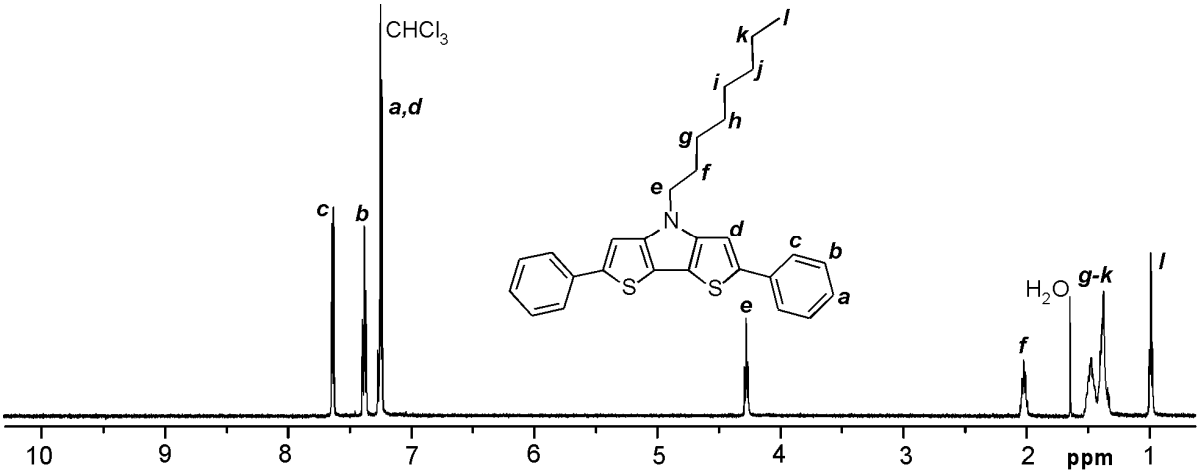

Figure S6. ^{1}H NMR Spectrum of Compound **12a**.

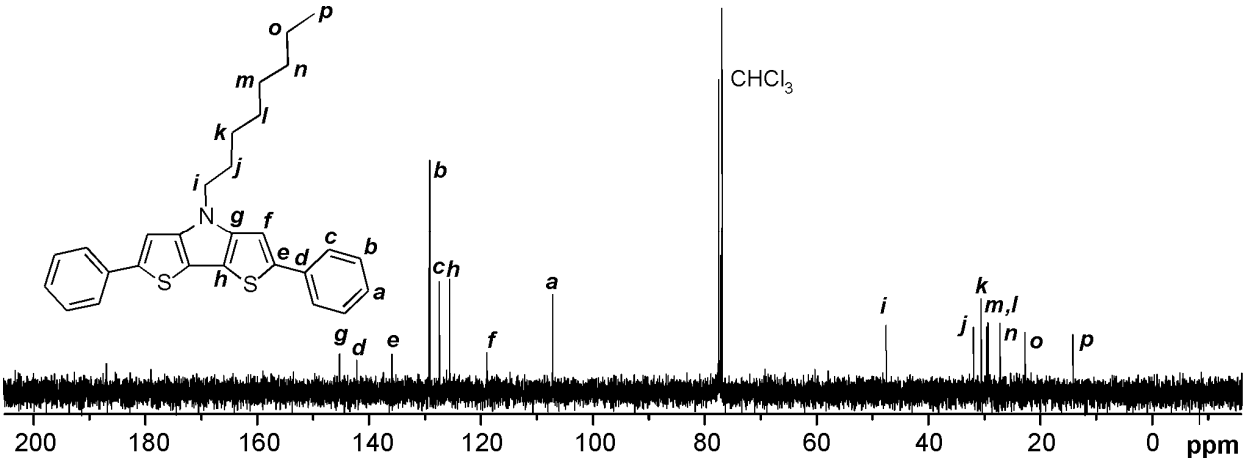

Figure S7. ^{13}C NMR Spectrum of Compound **12a**

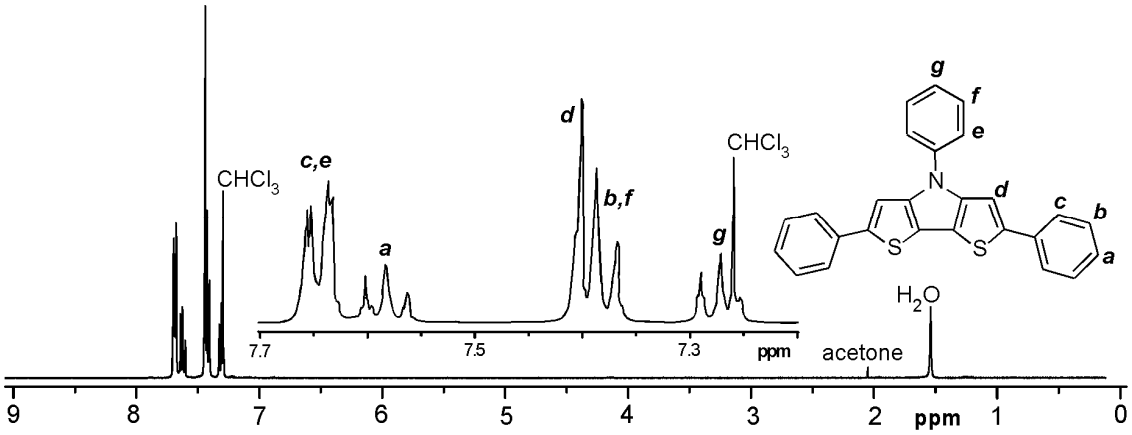

Figure S8. ^{1}H NMR Spectrum of Compound **12b**

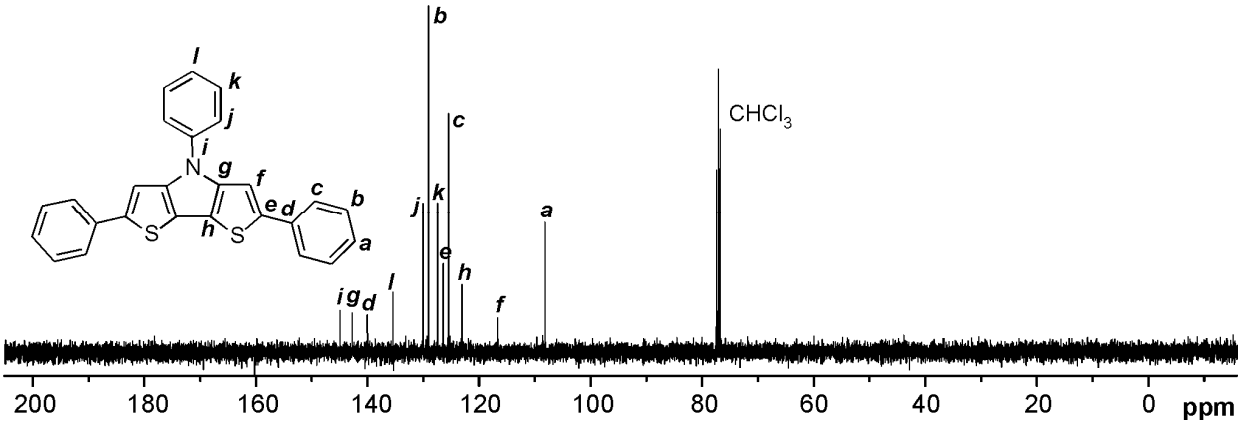

Figure S9. ^{13}C NMR Spectrum of Compound **12b**

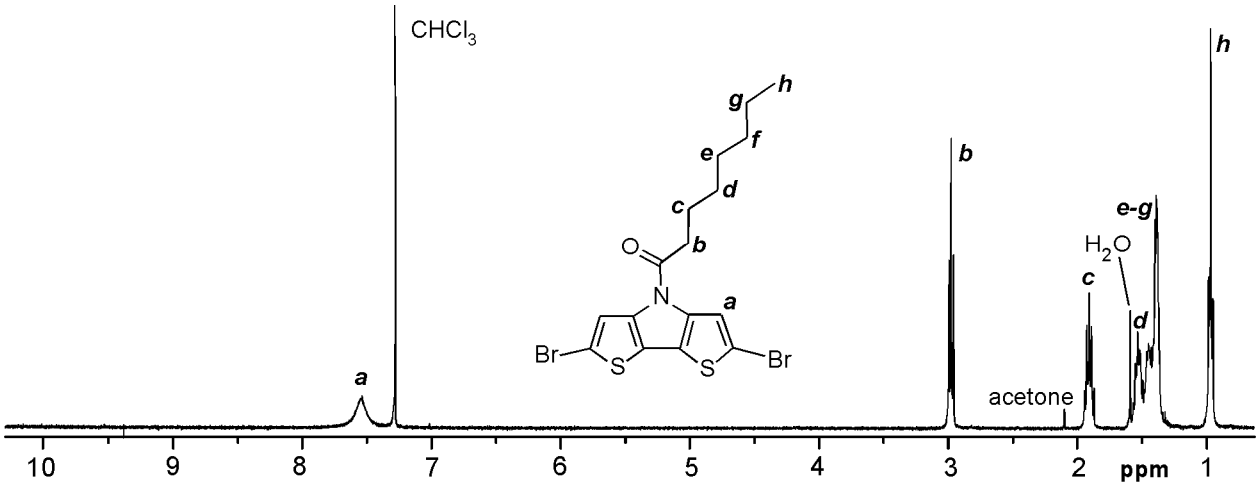

Figure S10. ^{1}H NMR Spectrum of Compound **15a**

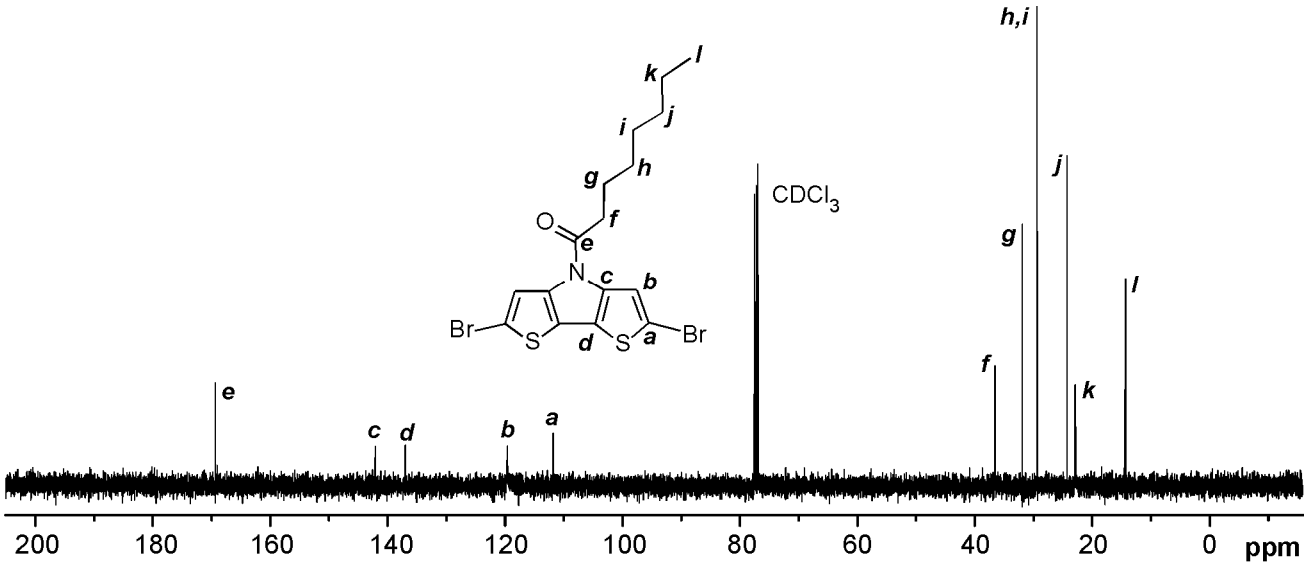

Figure S11. ^{13}C NMR Spectrum of Compound **15a**

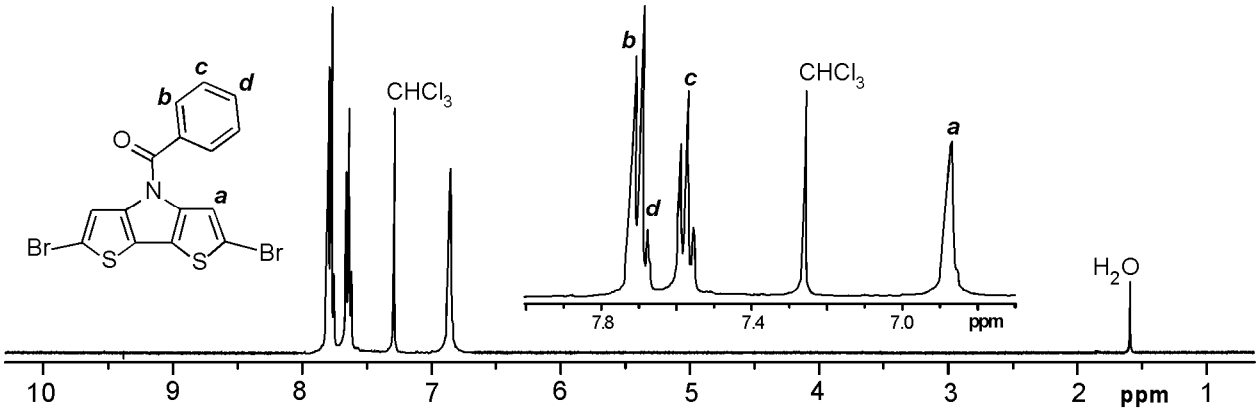

Figure S12. ^{1}H NMR Spectrum of Compound **15b**

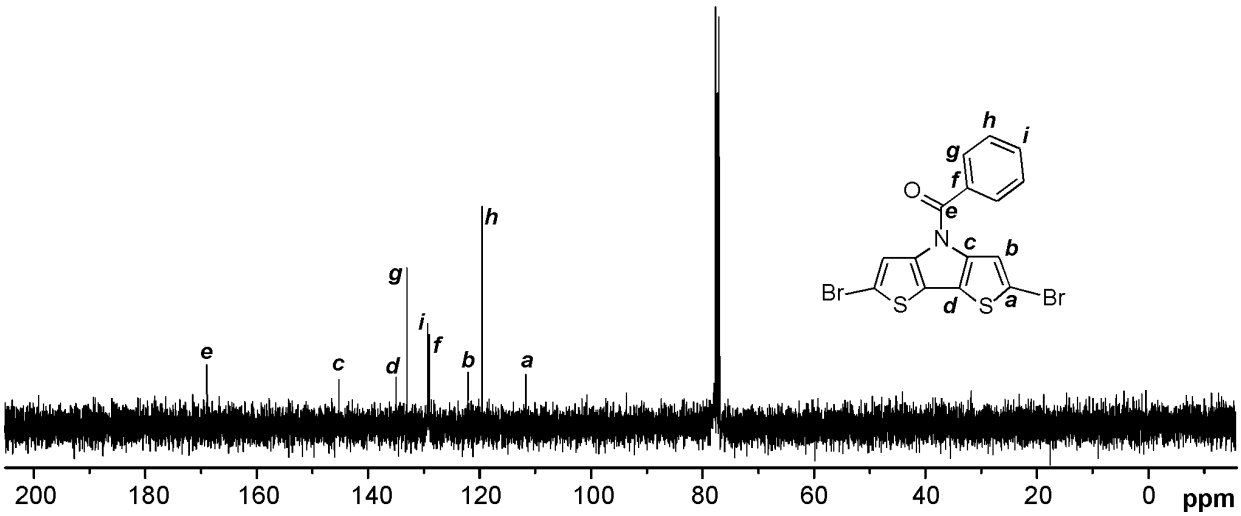

Figure S13. ^{13}C NMR Spectrum of Compound **15b**

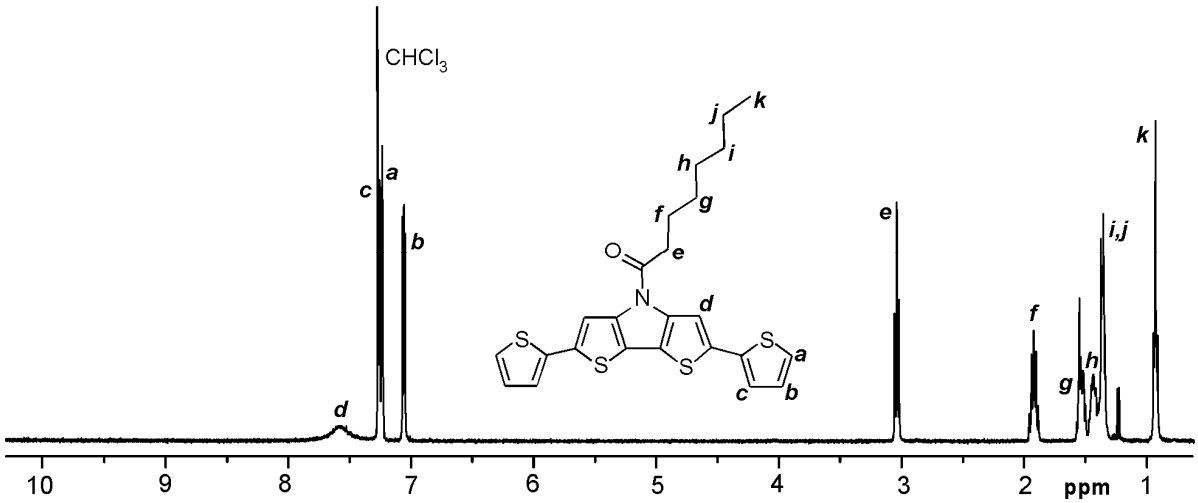

Figure S14. ^{1}H NMR Spectrum of Compound **8a**

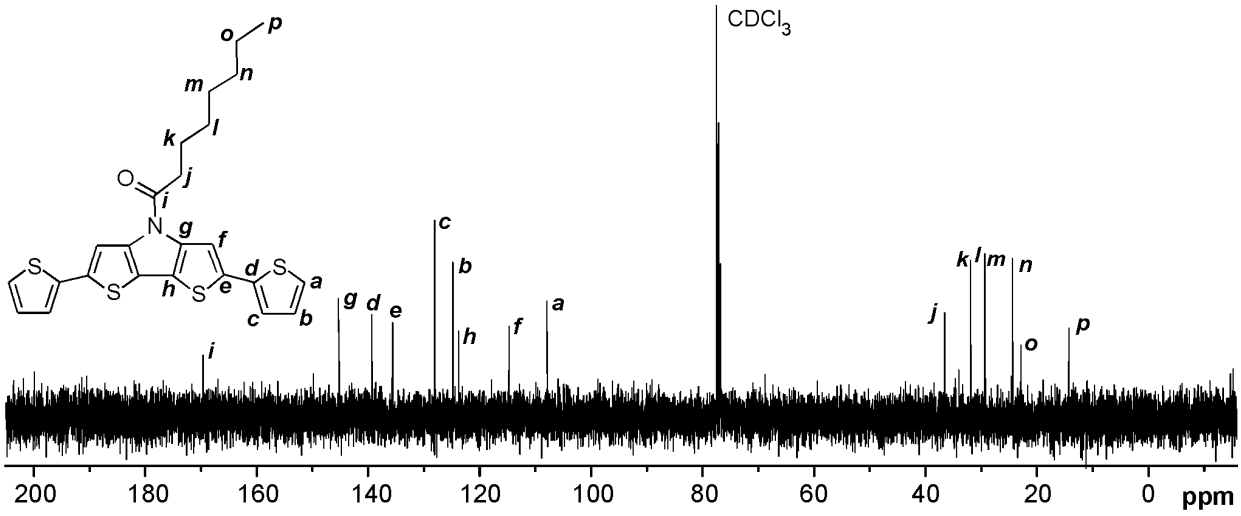

Figure S15. ^{13}C NMR Spectrum of Compound **8a**

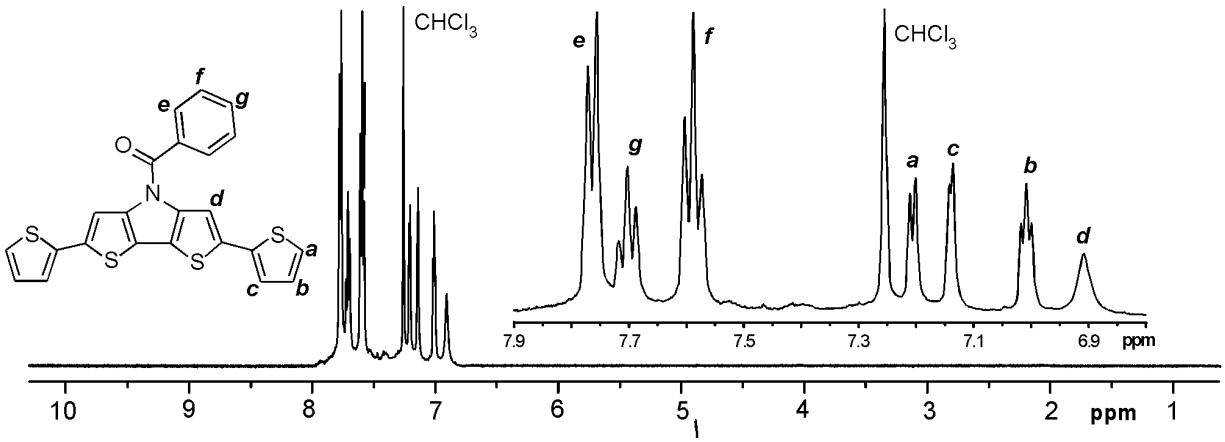

Figure S16. ^{1}H NMR Spectrum of Compound **8b**

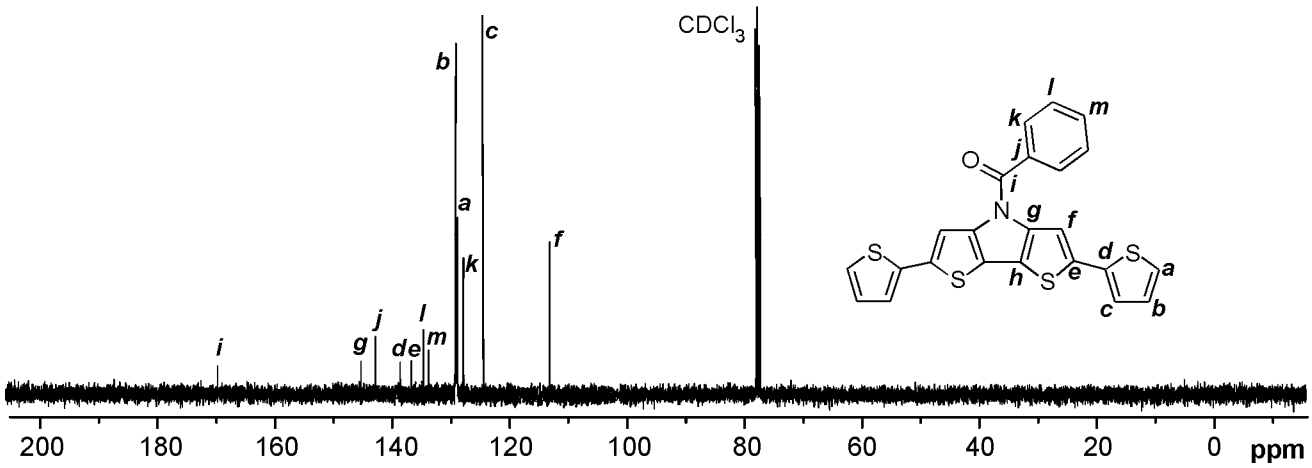

Figure S17. ^{13}C NMR Spectrum of Compound **8b**

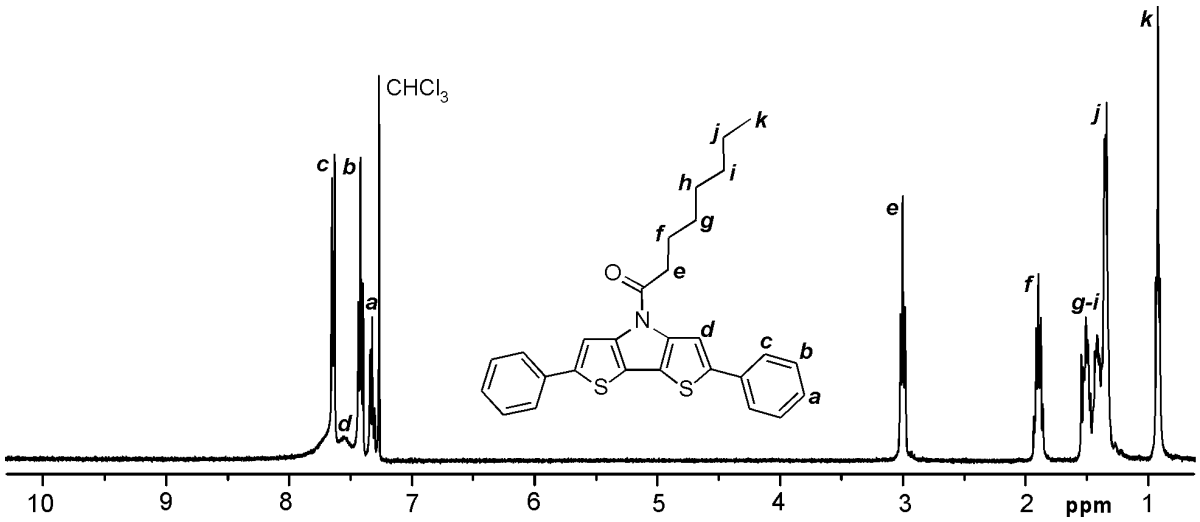

Figure S18. ^{1}H NMR Spectrum of Compound **13a**

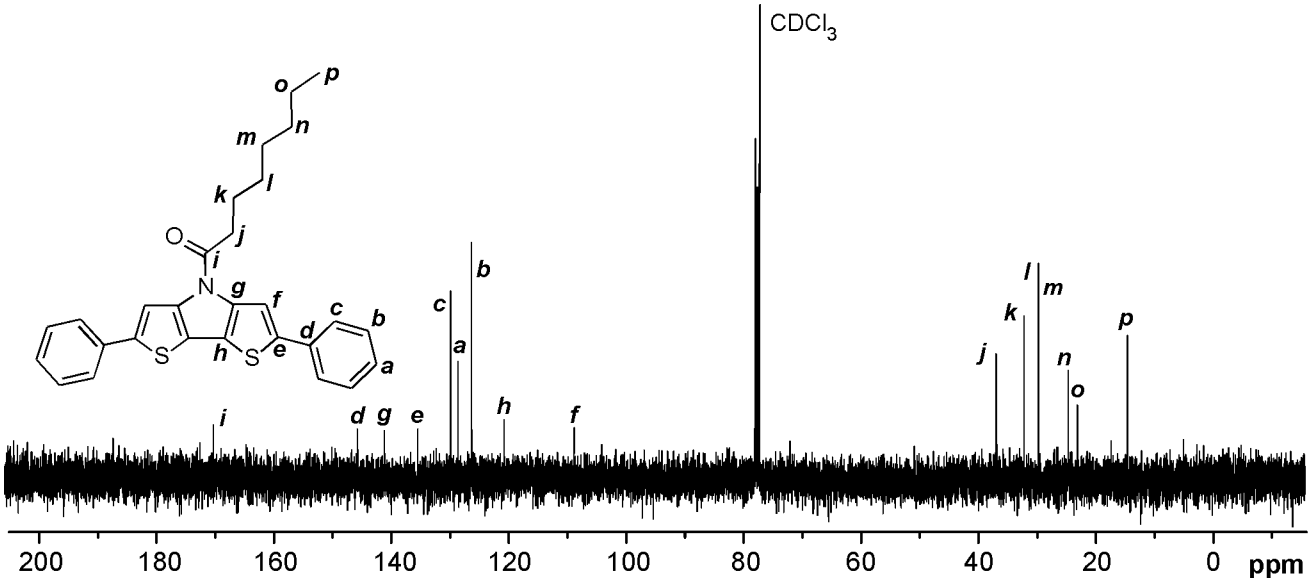

Figure S19. ^{13}C NMR Spectrum of Compound **13a**

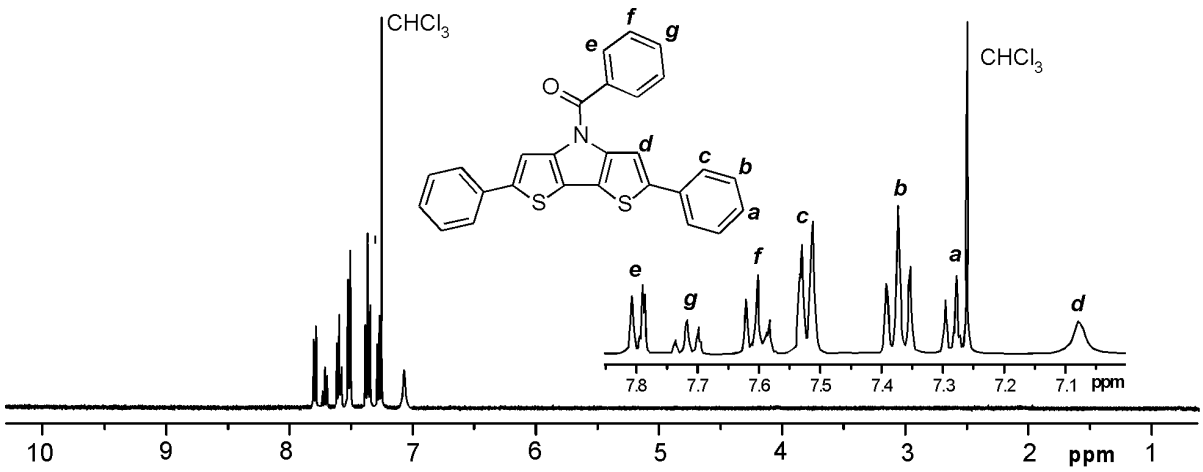

Figure S20. ^{1}H NMR Spectrum of Compound **13b**

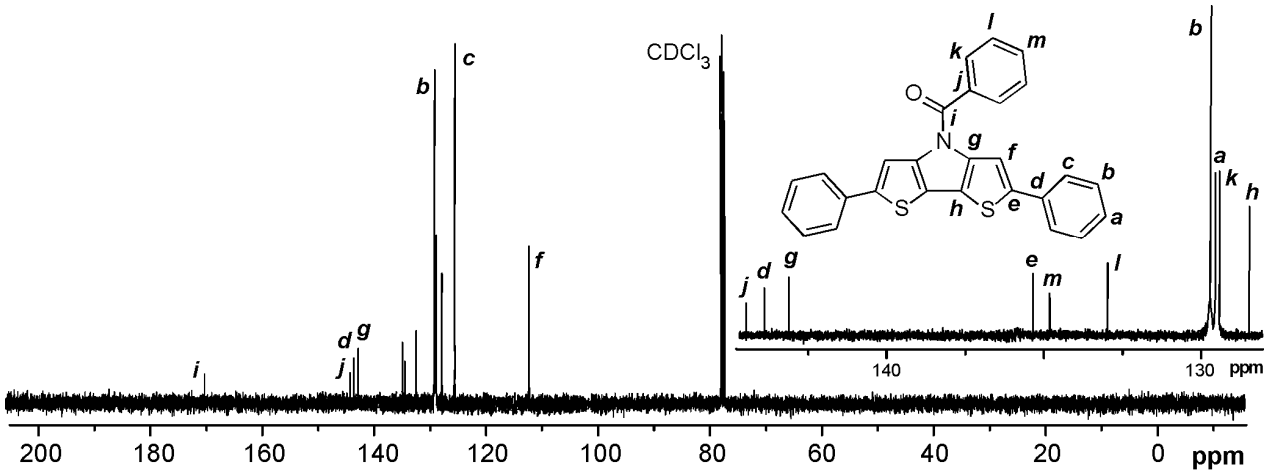

Figure S21. ^{13}C NMR Spectrum of Compound **13b**

X-ray Crystallography. X-ray quality crystals of **3b** and **7b** were grown by the slow evaporation of isopropanol solutions. Crystals of **15a** were grown from hexane solutions. The X-ray intensity data of the crystals were measured at 100 K on a Bruker Kappa Apex II Duo CCD-based X-ray diffractometer system equipped with a Mo-target X-ray tube (λ = 0.71073 Å) operated at 2000 W of power. The detector was placed at a distance of 5.000 cm from the crystal and data collected via the Bruker APEX2 software package. The frames were integrated with the Bruker SAINT software package. The unit cell was determined and refined by least-squares upon the refinement of XYZ-centeroids of reflections above 20σ(I). The structure was refined using the Bruker SHELXTL (Version 5.1) Software Package. The crystal data, data collection parameters, and refinement statistics are listed in Table S1. Full crystallography data for compounds **3b**, **7b**, and **15a** are attached as a separate CIF file.

Table S2. Crystal data, collection parameters, and refinement statistics for **3b**, **7b**, and **15a**

	3b	**7b**	**15a**
Formula	$C_{14}H_9NS_2$	$C_{22}H_{13}NS_4$	$C_{16}H_{17}Br_2NOS_2$
Formula Weight	255.34	419.57	463.25
Temperature (K)	100(2)	100(2)	100(2)
Crystal System	Monoclinic	Orthorhombic	Monoclinic
Space Group	P2(1)/c	Pna2(1)	P2(1)/c
a (Å)	9.9552(11)	10.8666(3)	8.9068(6)
b (Å)	14.2894(16)	22.8858(6)	21.4647(14)
c (Å)	8.1057(9)	7.4246(2)	9.5892(6)
α (º)	90.00	90.00	90.00
β (º)	101.783(2)	90.00	108.726(1)
γ (º)	90.00	90.00	90.00
V (Å^3)	1128.8(2)	1846.43(9)	1736.2(2)
Z	4	4	4
d_{calc} (g cm^{-3})	1.503	1.509	1.772
μ (mm^{-1})	0.443	4.774	4.910
Reflections collected	9952	6775	15990
Unique reflections	2707 [R_{int} = 0.0167]	2525 [R_{int} = 0.0292]	4003 [R_{int} = 0.0229]
Final R indices [I>2σ(I)]	R_1 = 0.0267	R_1 = 0.0306	R_1 = 0.0179
	wR_2 = 0.0699	wR_2 = 0.0796	wR_2 = 0.0416
R indices (all data)[a]	R_1 = 0.0298	R_1 = 0.0320	R_1 = 0.0218
	wR_2 = 0.0721	wR_2 = 0.0809	wR_2 = 0.0429
Goodness-of-fit on F^2	1.035	1.066	1.033

[a]$R_1 = \Sigma(||F_o| - |F_c||) / \Sigma|F_o|$, $wR_2 = [\Sigma(w(F_o^2 - F_c^2)^2) / \Sigma(F_o^2)^2]^{1/2}$, Goodness-of-fit on $F^2 = [\Sigma(w(F_o^2 - F_c^2)^2 / (n-p)]^{1/2}$, where n is the number of reflections and p is the number of parameters refined.

Theoretical Methodology. All calculations were performed with the Gaussian 03 program.[1] The molecular geometries of the neutral and radical-ion states were calculated at the Density Functional Theory (DFT) level using the B3LYP functional[2,3] and the 6-31G** basis[4-6] set. In all model compounds, long alkyl groups have been substitute by ethyl groups in **7** and **12** and by methyl groups **8** and **13**. For all the calculated molecules, frequency analyses were carried out to verify the nature of the minimum state of all the stationary points obtained by geometry optimization.The time-dependent DFT (TD-DFT) approach was used for the evaluation of the energies of the lowest singlet excited states.[7-9] The ionization potentials (IPs) and electron affinities (EAs) were calculated directly from the relevant points on the potential energy surfaces using the standard procedure detailed in the literature.10 Specifically, vertical IPs [EAs] were evaluated as the difference between the energy of the cation [anion] at the neutral geometry and that of the neutral species at the neutral geometry and adiabatic IPs [EAs] as the energy difference between the relaxed cation [anion] and the neutral molecule.

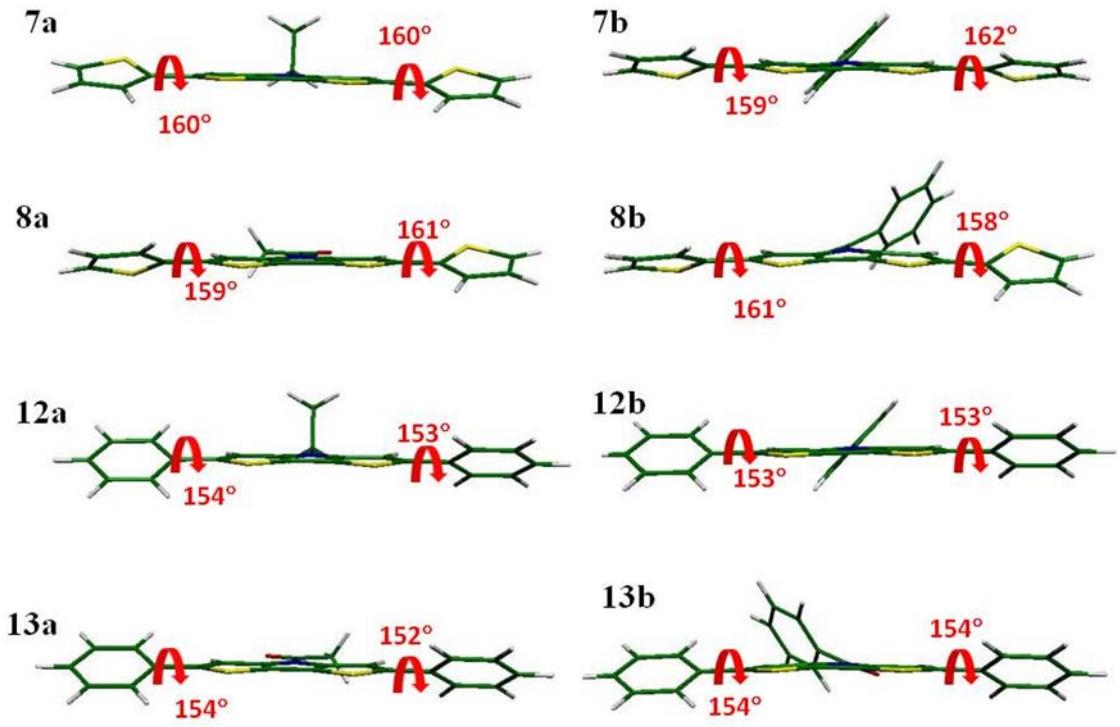

Figure S22. Lateral views of the optimum geometry of DTP-based oligomers in their neutral state computed at the B3LYP/6-31G** level. The calculated torsion angle θ defined around the central single bond linking the DTP unit and the external aromatic ring (i.e., thienyl or phenyl) is also shown.

Table S2. Summary of computed (DFT//B3LYP/6-31G**) frontier molecular orbital energies and HOMO-LUMO gaps for DTP-based oligomers and their related DTP monomers.

Compound	HOMO (eV)	LUMO (eV)	HOMO-LUMO gap (eV)
3a	-5.09	-0.55	4.54
3b	-5.21	-0.79	4.42
7a	-4.72	-1.59	3.13
7b	-4.79	-1.64	3.15
8a	-4.98	-1.90	3.08
8b	-4.93	-1.85	3.08
12a	-4.81	-1.35	3.46
12b	-4.89	-1.42	3.47
13a	-5.07	-1.71	3.36
13b	-5.04	-1.72	3.32

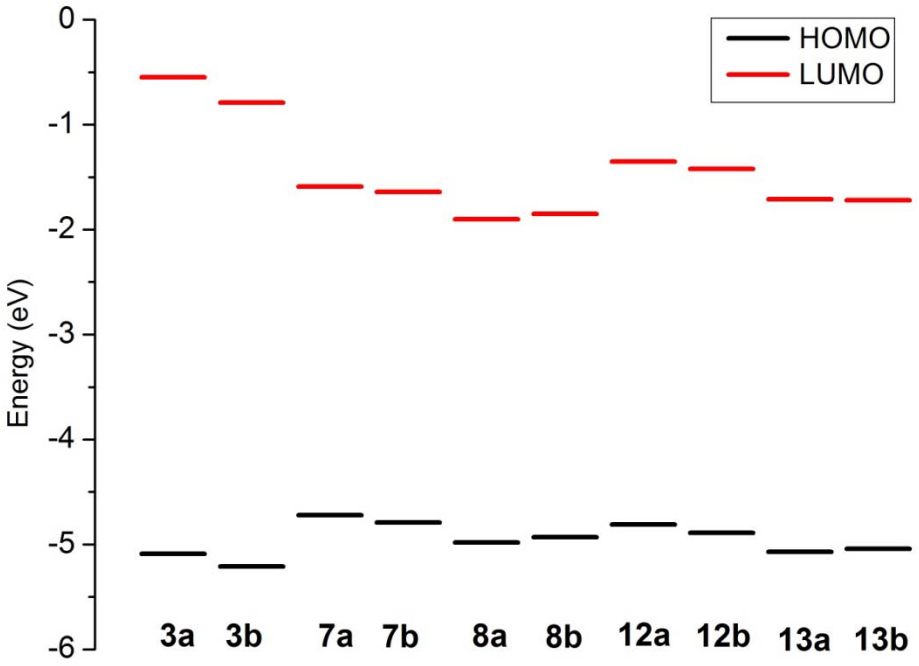

Figure S23. DFT//B3LYP/6-31G** absolute energies for the frontier molecular orbitals in DTP-based oligomers and their related DTP monomers.

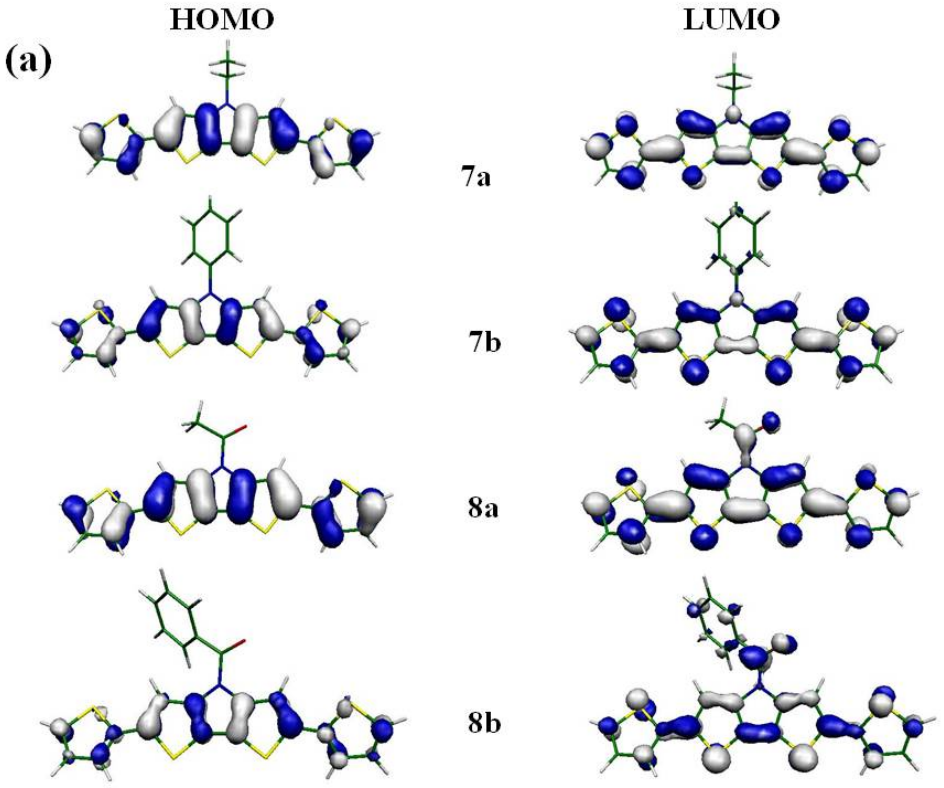

Figure S24. DFT//B3LYP/6-31G** electron density contours for 2,6-bis(2-thienyl)-substituted DTPs.

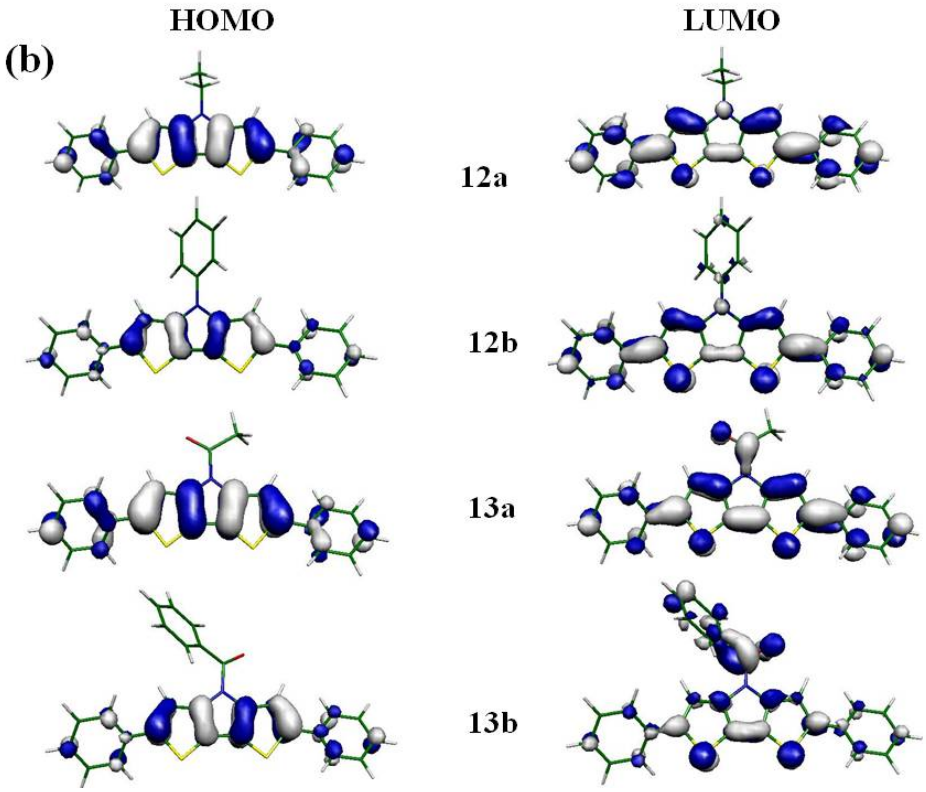

Figure S25. DFT//B3LYP/6-31G** electron density contours for 2,6-bis(phenyl)-substituted DTPs.

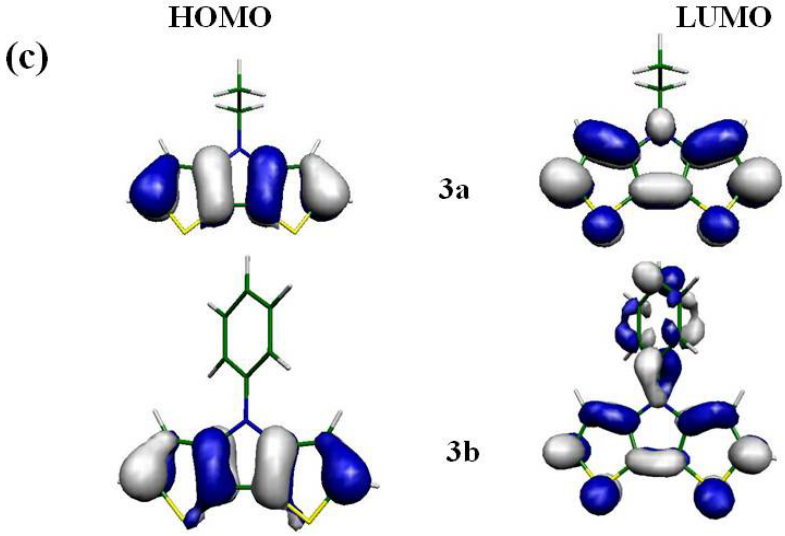

Figure S26. DFT//B3LYP/6-31G** electron density contours for DTPs **3a** and **3b**.

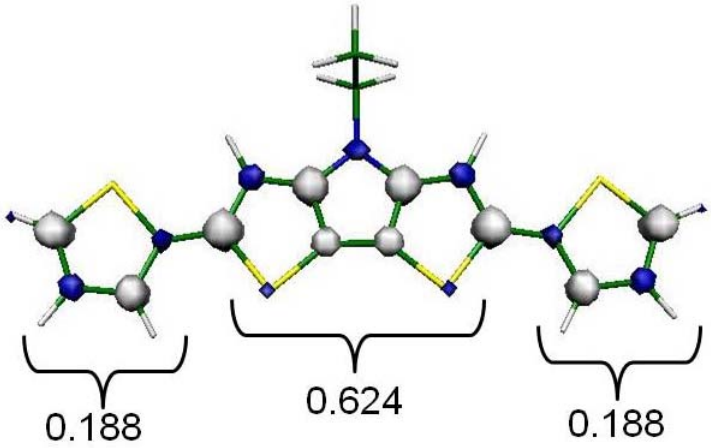

Figure S27. Isovalent surfaces (0.004 e/bohr^3) of spin electron density in **7a**. The summation of the atomic electron spin densities for the external thienyl rings and the central DTP-unit are given in electron.

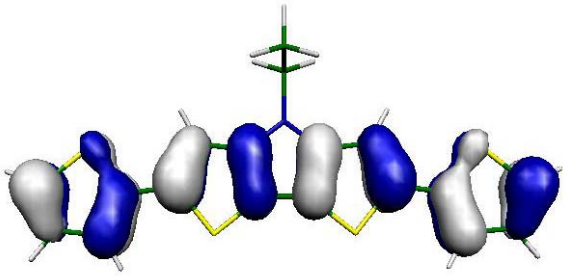

Figure S28. Singly occupied molecular orbital (SOMO) for the cation radical of **7a.**

Table S3. First ionization potentials (IPs) and electron affinities (EAs) for the DTP-based oligomers and their related DTP monomers obtained from ΔSCF and KT calculations at the B3LYP/6-31G** level.[a]

Compound	IP [eV]			EA[a] [eV]		
	vertical	adiabatic	Koopmans	vertical	adiabatic	Koopmans
3a	6.83	6.66	5.09	1.11	0.93	0.55
3b	6.88	6.67	5.21	0.68	0.51	0.79
7a	6.01	5.84	4.72	-0.35	-0.52	1.59
7b	6.04	5.85	4.79	-0.44	-0.64	1.64
8a	6.26	6.06	4.98	-0.65	-0.82	1.90
8b	6.18	5.97	4.93	-0.67	-0.81	1.85
12a	6.11	5.97	4.81	-0.13	-0.37	1.35
12b	6.15	5.98	4.89	-0.23	-0.49	1.42
13a	6.38	6.21	5.07	-0.47	-0.69	1.71
13b	6.30	6.12	5.04	-0.53	-0.71	1.72

[a] We have used the definition of EA as the energy change for the process $M+e^- \rightarrow M^{\bullet-}$; hence, the negative values indicate exothermicity for the reduction of a molecule.

Table S4. Intramolecular reorganization energies for hole (λh) and electron (λe) transfer in the DTP-based oligomers and their related DTP monomers, calculated at the B3LYP/6-31G** level.

Compound	λ_h	λ_e
3a	341	531
3b	412	636
7a	306	311
7b	347	343
8a	356	300
8b	376	260
12a	269	410
12b	316	446
13a	329	387
13b	345	323

References

1. Gaussian 03, Revision C.02, Frisch, M. J.; Trucks, G. W.; Schlegel, H. B.; Scuseria, G. E.; Robb, M. A.; Cheeseman, J. R.; Montgomery, Jr., J. A.; Vreven, T.; Kudin, K. N.; Burant, J. C.; Millam, J. M.; Iyengar, S. S.; Tomasi, J.; Barone, V.; Mennucci, B.; Cossi, M.; Scalmani, G.; Rega, N.; Petersson, G. A.; Nakatsuji, H.; Hada, M.; Ehara, M.; Toyota, K.; Fukuda, R.; Hasegawa, J.; Ishida, M.; Nakajima, T.; Honda, Y.; Kitao, O.; Nakai, H.; Klene, M.; Li, X.; Knox, J. E.; Hratchian, H. P.; Cross, J. B.; Bakken, V.; Adamo, C.; Jaramillo, J.; Gomperts, R.; Stratmann, R. E.; Yazyev, O.; Austin, A. J.; Cammi, R.; Pomelli, C.; Ochterski, J. W.; Ayala, P. Y.; Morokuma, K.; Voth, G. A.; Salvador, P.; Dannenberg, J. J.; Zakrzewski, V. G.; Dapprich, S.; Daniels, A. D.; Strain, M. C.; Farkas, O.; Malick, D. K.; Rabuck, A. D.; Raghavachari, K.; Foresman, J. B.; Ortiz, J. V.; Cui, Q.; Baboul, A. G.; Clifford, S.; Cioslowski, J.; Stefanov, B. B.; Liu, G.; Liashenko, A.; Piskorz, P.; Komaromi, I.; Martin, R. L.; Fox, D. J.; Keith, T.; Al-Laham, M. A.; Peng, C. Y.; Nanayakkara, A.; Challacombe, M.; Gill, P. M. W.; Johnson, B.; Chen, W.; Wong, M. W.; Gonzalez, C.; and Pople, J. A.; Gaussian, Inc., Wallingford CT, 2004.
2. Becke, A. D. *J. Chem. Phys.* **1993**, *98*, 5648.
3. Lee, C. T.; Yang, W. T.; Parr, R. G. *Phys. Rev. B* **1988**, *37*, 785.
4. Harihara, P. C.; Pople, J. A. *Theor. Chim. Acta* **1973**, *28*, 213.
5. Hehre, W. J.; Ditchfield, R.; Pople, J. A. *J. Chem. Phys.* **1972**, *56*, 2257.
6. Francl, M. M.; Pietro, W. J.; Hehre, W. J.; Binkley, J. S.; Gordon, M. S.; Defrees, D. J.; Pople, J. A. *J. Chem. Phys.* **1982**, *77*, 3654.
7. Runge, E.; Gross, E. K. U. *Phys. Rev. Lett.* **1984**, *52*, 997.
8. Gross, E. K. U.; Kohn, W. *Adv. Quantum Chem.* **1990**, *21*, 255.
9. Heinze, H.; Goerling, A.; Roesch, N. *J. Chem. Phys.* **2000**, *113*, 2088
10. Brédas, J. L.; Beljonne, D.; Coropceanu, V.; Cornil, *J. Chem. Rev.* **2004**, *104*, 4971.